Vol. 36 (2005) ACTA PHYSICA POLONICA B No 2

JET PRODUCTION AT HERA*

Claudia Glasman†

on behalf of the ZEUS and H1 Collaborations

Universidad Autónoma de Madrid, Depto. de Física Teórica
Cantoblanco 28049, Madrid, Spain

(Received October 5, 2004)

Recent results from jet production in deep inelastic ep scattering to investigate parton dynamics at low x are reviewed. The results on jet production in deep inelastic scattering and photoproduction used to test perturbative QCD are discussed and the values of $\alpha_{\rm s}(M_Z)$ extracted from a QCD analysis of the data are presented.

PACS numbers: 13.87.–a, 13.87.Ce

1. Introduction

Jet production in neutral-current (NC) deep inelastic ep scattering (DIS) and photoproduction provide tests of perturbative QCD (pQCD) calculations. Jet cross sections allow the determination of the fundamental parameter of QCD, the strong coupling constant $\alpha_{\rm s}$, and help to constrain the parton distribution functions (PDFs) in the proton.

Up to leading order (LO) in $\alpha_{\rm s}$, jet production in NC DIS proceeds via the quark–parton model ($Vq \rightarrow q$, where $V = \gamma^*$ or Z^0), boson–gluon fusion ($Vg \rightarrow q\bar{q}$) and QCD-Compton ($Vq \rightarrow qg$) processes. The jet production cross section is given in pQCD by the convolution of the proton PDFs and the subprocess cross section.

The main source of jets at HERA is hard scattering in photon–proton (photoproduction) interactions in which a quasi-real photon ($Q^2 \approx 0$, where Q^2 is the virtuality of the photon) emitted by the electron beam interacts with a parton from the proton to produce two jets in the final state. In LO QCD, there are two processes which contribute to the jet photoproduction

---
* Presented at the XXXIV International Symposium on Multiparticle Dynamics, Sonoma County, California, USA, July 26–August 1, 2004.

† Ramón y Cajal Fellow.

cross section: the resolved process, in which the photon interacts through its partonic content, and the direct process, in which the photon interacts as a point-like particle. The jet production cross section is given by the convolution of the flux of photons in the electron, the parton densities in the proton, the parton densities in the photon and the subprocess cross section.

At high scales, calculations using the DGLAP evolution equations have been found to give a good description of the data up to next-to-leading order (NLO). Therefore, by fitting the data with these calculations, it has been possible to extract accurate values of α_s and the gluon density of the proton. Most of these measurements refer to the production of jets irrespective of their partonic origin — quarks or gluons — and, therefore, have provided general tests of the partonic structure of the short-distance process and of combinations of the proton and/or photon PDFs. The identification of quark and gluon jets would allow more stringent tests of the QCD predictions.

2. Parton evolution at low Bjorken-x

To leading logarithm accuracy, the DGLAP evolution is equivalent to the exchange of a parton cascade with the exchanged partons strongly ordered in virtuality. The DGLAP equations sum the leading powers of $\alpha_s \log Q^2$ in the region of strongly-ordered transverse momenta. However, DGLAP evolution is expected to breakdown at low x since terms proportional to $\alpha_s \log 1/x$ are neglected.

Several theoretical approaches exist which account for low-x effects not incorporated into the DGLAP evolution. They are: *(i)* the BFKL equations, which resum $\log(1/x)$ terms and exhibit no k_T ordering; *(ii)* the CCFM equations incorporate angular-ordered parton emission and are equivalent to BFKL for $x \to 0$ and to DGLAP at large x; *(iii)* the introduction of a second k_T-ordered parton cascade on the photon side à la DGLAP, which is implemented by assigning a partonic structure to the virtual photon, mimics higher-order QCD effects at low x.

These approaches to low-x dynamics have been incorporated into models: Ariadne, which generates non-k_T ordered parton cascades based on the color dipole model (CDM); Cascade, which is based on the CCFM equations; and Rapgap, in which direct processes can be supplemented with resolved processes in $\gamma^* p$ interactions. For comparison, predictions based on the DGLAP equations have been performed using either the programs Disent and Nlojet, which provide fixed-order pQCD calculations up to NLO, or Rapgap including only direct processes, in which higher-order effects are implemented in a leading-logarithm parton-shower approach.

Experimentally, deviations from the DGLAP evolution can be expected at low x and forward-jet rapidity since parton emission along the exchanged gluon ladder increases with decreasing x. Another method to obtain evidence for DGLAP breakdown is to study the azimuthal correlation between the two hardest jets. In DGLAP, partons entering the hard process with negligible $k_{\rm T}$ produce a back-to-back configuration at LO. Values of $\Delta\phi < 180°$ occur in DGLAP due to higher-order QCD effects. In models which predict a significant proportion of partons entering the hard process with large $k_{\rm T}$, the number of events with small $\Delta\phi$ will increase.

2.1. x dependence of the forward-jet cross section

The forward-jet cross section has been measured [1] for jets identified with the $k_{\rm T}$ cluster algorithm in the longitudinally inclusive mode in the laboratory frame. Events with at least one jet of $E^{\rm jet}_{\rm T,LAB} > 3.5$ GeV and $1.7 < \eta^{\rm jet}_{\rm LAB} < 2.8$ were selected. The events are required to fulfill the additional conditions: $x_{\rm jet} = E_{\rm jet}/E_p > 0.035$, where E_p is the proton-beam energy, and $0.5 < (E^{\rm jet}_{\rm T})^2/Q^2 < 5$, following the proposal of Mueller and Navelet to allow evolution in x and to restrict evolution in Q^2. The measurements were made in the kinematic region given by $5 < Q^2 < 85$ GeV^2 and $0.0001 < x < 0.004$.

Figure 1 shows the forward-jet cross section as a function of x. The measured cross section rises with decreasing x. The NLO calculation corrected for hadronisation effects obtained using the program Disent with $\mu^2_{\rm R} = \langle (E^{\rm jet}_{\rm T})^2 \rangle = 45$ GeV^2 and the CTEQ6 proton PDFs, is compared to the data in Fig. 1(a). The measured cross section is well described by the

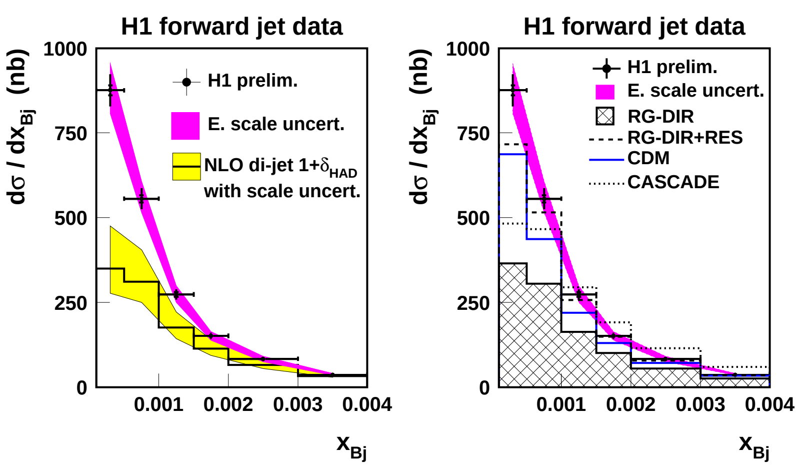

(a) (b)

Fig. 1. Forward-jet cross section [1] and the predictions of (a) Disent and (b) Rapgap (RG), Ariadne (CDM) and Cascade.

prediction for large values of x, but at low x values there is a large excess of data with respect to the calculation. This prediction is based on DGLAP evolution and so it is not expected to work in this region of phase space. Figure 1(b) shows the comparison with the predictions of different Monte Carlo models. The prediction of RAPGAP including only direct processes is similar to the NLO calculation. Once the contribution from resolved processes is included, a better description of the data is obtained for x down to 0.001. The CASCADE prediction does not reproduce the shape of the data, whereas the prediction from CDM describes the data for $x > 0.0015$. In conclusion, no model can describe the sharp rise of the data at very low x.

2.2. Azimuthal jet separation

The azimuthal correlation between the two hard jets in dijet events has been measured [2] using the k_{T}-cluster algorithm in the longitudinally inclusive mode in the $\gamma^* p$ centre-of-mass frame. The measurements were made in the kinematic region given by $5 < Q^2 < 100$ GeV^2 and $10^{-4} < x < 10^{-2}$. The cross sections refer to jets of $E_{\mathrm{T}}^* > 5$ GeV, $-1 < \eta_{\mathrm{LAB}}^{\mathrm{jet}} < 2.5$ and $E_{\mathrm{T,max}}^* > 7$ GeV, where E_{T}^* is the jet transverse energy in the $\gamma^* p$ centre-of-mass frame. The fraction S of the number of dijet events with an azimuthal separation between $0°$ and $120°$ is presented in Fig. 2(a) as a function of x in different regions of Q^2. The data rise towards low x values, especially at low Q^2. The predictions from DISENT, which contain the lowest-order contribution to S, are several standard deviations below the data and show no dependence with x. On the other hand, the predictions of NLOJET, which incorporate NLO corrections to S, provide a good description of the data at large Q^2 and large x. However, they fail to describe the increase of the data towards low x values, especially at low Q^2. This shows the need to incorporate NLO corrections to the calculations.

Higher-order effects can be mimicked by the parton shower approach in Monte Carlo models. If the observed discrepancies are due to the influence of non-ordered parton emission, models based on the CDM or the CCFM evolution could provide a better description of the data. Figure 2(b) shows the data compared with ARIADNE, which gives a good description of the data at low x and Q^2, but fail to describe the data at high Q^2. The predictions of CASCADE using JS2001 lie significantly above the data in all x and Q^2 regions, whereas those using Jung2003 are closer to the data. Therefore, the measurement of the fraction S is sensitive to and can be used to gain information on the unintegrated parton distributions.

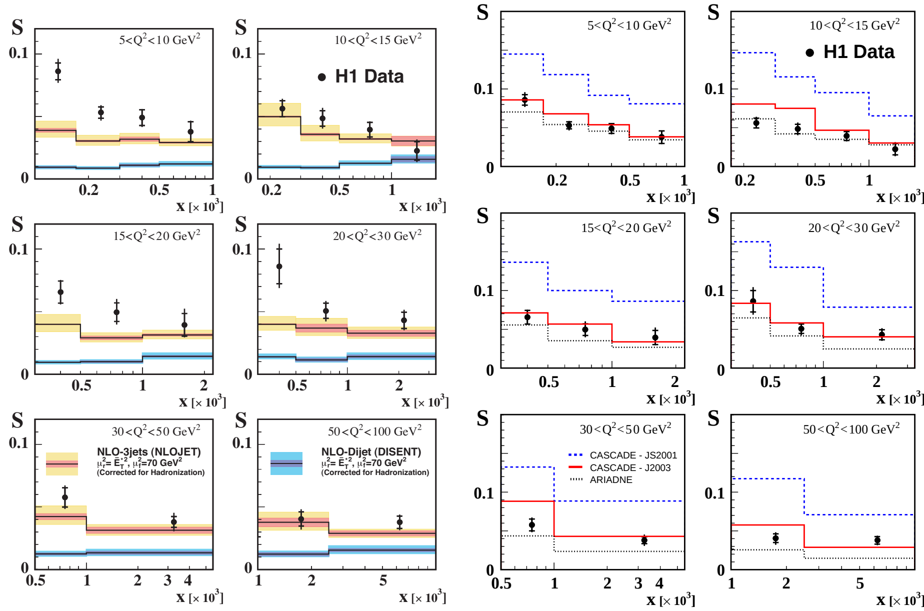

(a) (b)

Fig. 2. Fraction S as a function of x in different Q^2 regions [2] and the predictions of the calculations from (a) Disent and Nlojet and (b) Cascade and Ariadne.

3. Multi-jet production in NC DIS

Three-jet production in NC DIS provides a test of pQCD directly beyond LO since the lowest-order contribution is proportional to α_s^2. Three-jet events arise from additional gluon brehmstrahlung or splitting of a gluon into a $q\bar{q}$ pair. The dijet (three-jet) cross section has been measured [3] using the k_T cluster algorithm in the longitudinally invariant mode in the Breit frame for events with at least two (three) jets of $E_{T,B}^{jet} > 5$ GeV and $-1 < \eta_{LAB}^{jet} < 2.5$, and with dijet (three-jet) invariant masses in excess of 25 GeV; the kinematic region is defined by $10 < Q^2 < 5000$ GeV^2. Figure 3(a) shows the dijet and three-jet cross sections as functions of Q^2. The data are compared to the predictions of Nlojet up to $\mathcal{O}(\alpha_s^2)$ and $\mathcal{O}(\alpha_s^3)$, respectively, using $\mu_R^2 = Q^2 + (\bar{E}_{T,B}^{jet})^2$, where $\bar{E}_{T,B}^{jet}$ is the average jet transverse energy of the two (three) jets, and $\mu_F = Q$. The CTEQ6 sets have been used for the proton PDFs. The measured cross sections are well described by the predictions.

The Q^2 dependence of the ratio of the three-jet to the dijet cross section has been studied (see Fig. 3(b)). Many experimental and theoretical

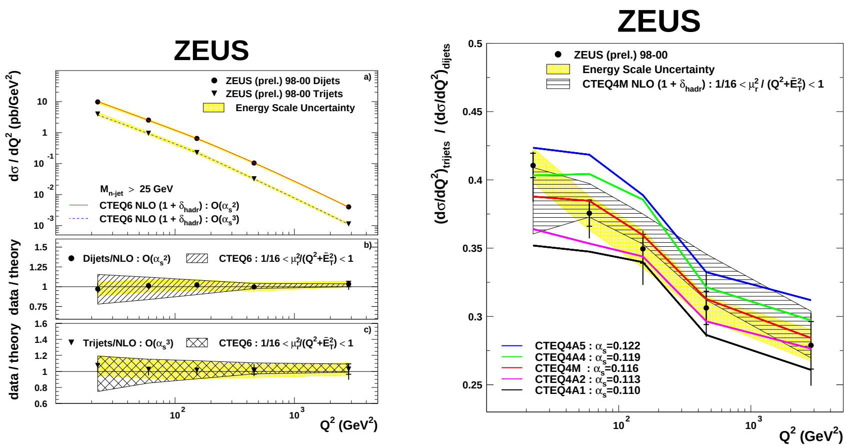

(a) **(b)**

Fig. 3. (a) Dijet and three-jet cross sections in NC DIS as a function of Q^2 [3]. (b) Ratio of the cross sections as a function of Q^2 [3] and the predictions of NLOJET.

uncertainties cancel in the ratio and therefore this observable provides a more accurate test of color dynamics, especially at low Q^2. The calculations from NLOJET, using the five sets of the CTEQ4 "A-series" of proton PDFs, give a good description of the data and show the sensitivity of this observable to the value of $\alpha_s(M_Z)$ assumed in the calculations. A value of $\alpha_s(M_Z) = 0.1179 \pm 0.0013$ (stat.) $^{+0.0028}_{-0.0046}$ (exp.) $^{+0.0061}_{-0.0047}$ (th.) has been extracted from the ratio, which is in good agreement with the world average and other determinations of α_s from HERA data.

4. Jet substructure and the dynamics of quarks and gluons

The internal structure of a jet depends mainly on the type of primary parton from which it originated and to a lesser extent on the particular hard scattering process. QCD predicts that at sufficiently high $E_T^{\rm jet}$, where fragmentation effects become negligible, the jet structure is driven by gluon emission off the primary parton and is then calculable in pQCD. QCD also predicts that gluon jets are broader than quark jets due to the larger color charge of the gluon.

The internal structure of jets has been studied by means of the mean integrated jet shape, which is defined as the fraction of the jet transverse energy that lies inside a cone in the $\eta - \varphi$ plane of radius r concentric with the jet axis, using only those particles belonging to the jet. The mean integrated jet shape, $\langle\psi(r)\rangle$, is defined as the averaged fraction of the jet transverse energy inside the cone of radius r.

The quark and gluon content of the final state has been investigated by studying the $\eta^{\rm jet}$ dependence of the jet shape in photoproduction and NC DIS at a fixed value of $r = 0.5$ (see Fig. 4(a)) [4]. The jets have been identified using the $k_{\rm T}$ cluster algorithm in the longitudinally inclusive mode and selected according to $E_{\rm T}^{\rm jet} > 17$ GeV and $-1 < \eta^{\rm jet} < 2.5$. The kinematic region in the photoproduction sample is defined by $Q^2 < 1$ GeV^2 and $142 < W_{\gamma p} < 293$ GeV, where $W_{\gamma p}$ is the γp centre-of-mass energy, and in the NC DIS sample by $Q^2 > 125$ GeV^2. The photoproduction data decreases with increasing $\eta^{\rm jet}$ for photoproduction, *i.e.* the jets become broader as $\eta^{\rm jet}$ increases. On the other hand, the jets in NC DIS show no dependence with $\eta^{\rm jet}$. The comparison of the data with the predictions for quark and gluon jets shows that the jets in NC DIS are consistent with being dominated by quark jets, whereas the broadening of the jets in photoproduction is consistent with an increase of the fraction of gluon jets as $\eta^{\rm jet}$ increases. The dependence of $\langle\psi(r = 0.5)\rangle$ as a function $E_{\rm T}^{\rm jet}$ (see Fig. 4(b)) in NC DIS shows that the jets become narrower as $E_{\rm T}^{\rm jet}$ increases. The comparison of the data with NLO calculations assuming different values of $\alpha_{\rm s}(M_Z)$ shows the sensitivity of this observable to the value of $\alpha_{\rm s}(M_Z)$. A value of $\alpha_{\rm s}(M_Z) = 0.1176 \pm 0.0009\ ({\rm stat.})\ ^{+0.0009}_{-0.0026}\ ({\rm exp.})\ ^{+0.0091}_{-0.0072}\ ({\rm th.})$ was determined from this observable.

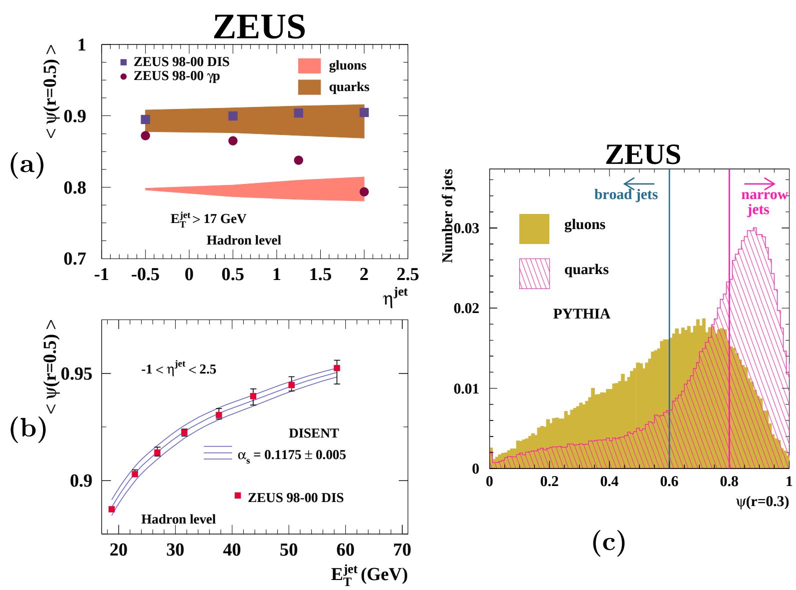

Fig. 4. (a) $\langle\psi(r = 0.5)\rangle$ as a function of $\eta^{\rm jet}$ in photoproduction and NC DIS [4] and the predictions for quark and gluon jets. (b) $\langle\psi(r = 0.5)\rangle$ as a function of $E_{\rm T}^{\rm jet}$ in NC DIS [4] and the predictions of Disent. (c) Predicted $\psi(r = 0.3)$ distributions for quark and gluon jets.

The predictions of the Monte Carlo for the jet shape reproduce well the data and show the expected differences for quark and gluon jets. These differences were used to select samples enriched in quark and gluon jets to study in more detail the dynamics of the hard subprocesses. The predicted shapes of the distribution in $\psi(r = 0.3)$ for quark and gluon jets are different, as shown in Fig. 4(c). A sample enriched in quark (or "narrow") jets was selected by requiring $\psi(r = 0.3) > 0.8$ and a sample enriched in gluon (or "broad") jets was selected by requiring $\psi(r = 0.3) < 0.6$.

The inclusive-jet cross-section $d\sigma/d\eta^{\rm jet}$ for photoproduction is shown in Fig. 5(a) for samples of broad and narrow jets. The measured cross sections exhibit different behaviors: the $\eta^{\rm jet}$ distribution for broad jets increases up to the highest $\eta^{\rm jet}$ value measured, whereas the distribution for narrow jets peaks at $\eta^{\rm jet} \approx 0.7$. Predictions from Pythia are compared to the measurements in Fig. 5(a). The same selection method was applied to the Monte Carlo jets. The predictions provide a good description of the shape of the narrow-jet distribution in the data. The shape of the broad-jet distribution in the data is reasonably well described by Pythia. Figure 5(a) also shows the predictions of Pythia for jets of quarks and gluons separately. These predictions have been obtained without any selection. The calculation that includes only quark (gluon) jets gives a reasonable description of the narrow (broad)-jet cross section. This result supports the expectation that the broad (narrow)-jet sample is dominated by gluon (quark) jets.

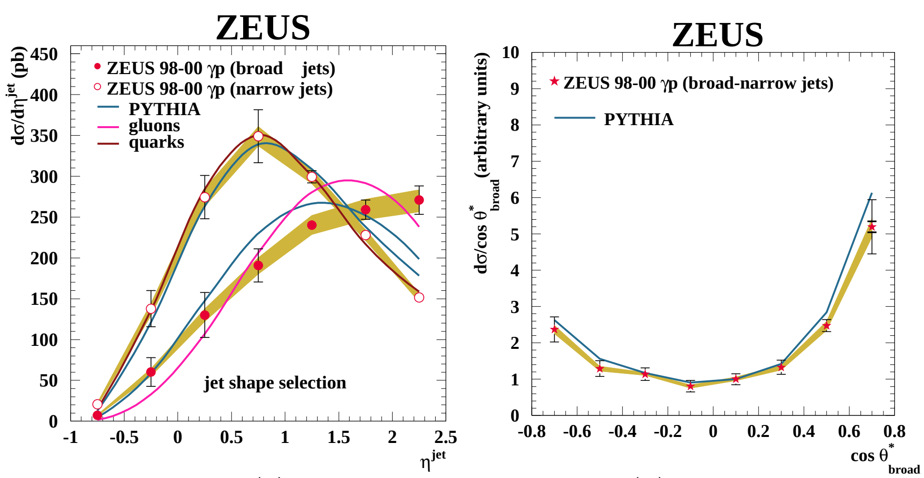

(a) (b)

Fig. 5. (a) Measured inclusive-jet cross section in photoproduction as a function of $\eta^{\rm jet}$ for samples of broad and narrow jets [4]. (b) Measured dijet cross section in photoproduction as a function of $\cos\theta^*_{\rm broad}$ [4] and the predictions of Pythia.

The distribution in θ^*, where θ^* is the angle between the jet–jet axis and the beam direction in the dijet system, reflects the underlying parton dynamics and is sensitive to the spin of the exchanged particle. In the case of direct-photon interactions, the contributing subprocesses at LO QCD involve quark exchange and so $d\sigma/d|\cos\theta^*| \propto (1-|\cos\theta^*|)^{-1}$ as $|\cos\theta^*| \to 1$. In the case of resolved-photon interactions, the dominant subprocesses are those that involve gluon exchange and $d\sigma/d|\cos\theta^*| \propto (1-|\cos\theta^*|)^{-2}$ as $|\cos\theta^*| \to 1$. The sample of dijet events with one broad jet and one narrow jet was used to measure $d\sigma/d\cos\theta^*_{\rm broad}$, where $\theta^*_{\rm broad}$ refers to the angle with respect to the broad jet. Figure 5(b) shows the measured cross section. The distribution shows a different behavior on the negative and positive sides; the measured cross section at $\cos\theta^*_{\rm broad} = 0.7$ is approximately twice as large as at $\cos\theta^*_{\rm broad} = -0.7$. The calculation from PYTHIA gives a good description of the shape of the measured $d\sigma/d\cos\theta^*_{\rm broad}$. The observed asymmetry is understood in terms of the dominant resolved subprocess $q_\gamma g_p \to qg$. The $\cos\theta^*_{\rm broad}$ distribution for this subprocess is asymmetric due to the different dominant diagrams in the regions $\cos\theta^*_{\rm broad} \to +1(-1)$: $t(u)$-channel gluon (quark) exchange. In conclusion, the hard subprocesses have been investigated separately in photoproduction for the first time using the internal structure of jets.

5. Conclusions

HERA has become a unique QCD-testing machine. At large scales considerable progress in understanding and reducing the uncertainties has led to very precise determinations of $\alpha_{\rm s}$ as well as further insight into the dynamics of quarks and gluons. To achieve even better accuracy in the determination of $\alpha_{\rm s}$ and to fully understand the new regime of low x, further improvements in the QCD calculations are needed.

REFERENCES

[1] H1 Coll., Contributed paper N 5-0172 to the 32nd International Conference on High Energy Physics, August 16–22, 2004, Beijing.

[2] H1 Coll., A. Aktas *et al.*, *Eur. Phys. J.* **C33**, 477 (2004).

[3] ZEUS Coll., Contributed paper N 5-0294 to the 32nd International Conference on High Energy Physics, August 16–22, 2004, Beijing.

[4] ZEUS Coll., S. Chekanov *et al.*, DESY 04-072 and `hep-ex/0405065`.